Crystal Structure of Macrophage Migration Inhibitory Factor Complexed with (*E*)-2-Fluoro-*p*-hydroxycinnamate at 1.8 Å Resolution: Implications for Enzymatic Catalysis and Inhibition[†,‡]

Alexander B. Taylor, William H. Johnson, Jr., Robert M. Czerwinski, Horng-Shin Li, Marvin L. Hackert,* and Christian P. Whitman*

Department of Chemistry and Biochemistry, and Medicinal Chemistry Division, College of Pharmacy, The University of Texas, Austin, Texas 78712-1071

Received February 19, 1999; Revised Manuscript Received April 13, 1999

ABSTRACT: Macrophage migration inhibitory factor (MIF) exhibits dual activities. It acts as an immunoregulatory protein as well as a phenylpyruvate tautomerase. To understand better the relationship between these two activities and to elucidate the structural basis for the enzymatic activity, a crystal structure of a complex between murine MIF and (*E*)-2-fluoro-*p*-hydroxycinnamate, a competitive inhibitor of the tautomerase activity, has been determined to 1.8 Å resolution. The structure is nearly superimposable on that of the free protein indicating that the presence of the inhibitor does not result in any major structural changes. The inhibitor also confirms the location of the active site in a hydrophobic cavity containing the amino-terminal proline. Within this cavity, the inhibitor interacts with residues from adjacent subunits. At the back of the cavity, the side-chain carbonyl oxygen of Asn-97′ interacts with the phenolic hydroxyl group of the inhibitor while at the mouth of the cavity the ammonium group of Lys-32 interacts with a carboxylate oxygen. The other carboxylate oxygen of the inhibitor interacts with Pro-1. The hydroxyl group of Tyr-95′ interacts weakly with the fluoro group on the inhibitor. The hydrophobic side chains of five active-site residues (Met-2, Ile-64, Met-101, Val-106, and Phe-113) and the phenyl moiety of Tyr-95′ are responsible for the binding of the phenyl group. Further insight into the enzymatic activity of MIF was obtained by carrying out kinetic studies using the enol isomers of phenylpyruvate and (*p*-hydroxyphenyl)pyruvate. The results demonstrate that MIF processes the enol isomers more efficiently than the keto isomers primarily because of a decrease in K_m. On the basis of these results, a mechanism is proposed for the MIF-catalyzed tautomerization reaction.

Macrophage migration inhibitory factor (MIF)[1] has emerged as an important regulatory protein in the immune system which may be involved in the pathogenesis of a variety of inflammatory conditions (*1*−*3*). The preformed protein is released into circulation in response to elevated levels of glucocorticoids resulting from biological stress or the presence of bacterial lipopolysaccharide (LPS). It acts by an unknown mechanism as a proinflammatory mediator to counteract the antiinflammatory effects of glucocorticoids and thereby controls local and systemic immune responses (*1*). Recently, it has been shown that MIF catalyzes the enolization of phenylpyruvate (**1** → **2**, Scheme 1) and (*p*-hydroxyphenyl)pyruvate (**3** → **4**, Scheme 1) (*4*). The identification of these substrates, western blot analysis using an antibody to MIF, and the fact that the amino-terminal 15 amino acids of the commercially available phenylpyruvate tautomerase (PPT) are identical to those of bovine MIF led to the conclusion that MIF and PPT are the same protein (*4*). It is not yet clear how or if this phenylpyruvate tautomerase activity is related to any of the immunological or inflammatory activities of MIF.

Scheme 1

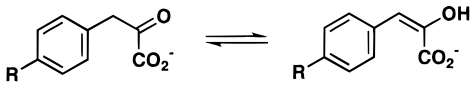

1: R=H **2: R=H**

3: R=OH **4: R=OH**

A fundamental aspect of the catalytic strategy used in MIF's enzymatic activity was uncovered when it was found that the crystal structures of both the rat liver and human MIF are superimposable on those of two bacterial isomerases,

[†] This research was supported by the National Institutes of Health Grant GM-41239, the Texas Advanced Research Program (ARP-183), the Robert A. Welch Foundation (F-1334) to C.P.W., and the National Institutes of Health Grant GM-30105 and the Robert A. Welch Foundation (F-1219) to M.L.H.

[‡] The coordinates have been deposited with the Brookhaven Protein Data Bank (PDB code 1MFI).

* To whom correspondence should be addressed. (M.L.H.) Phone: (512) 471-3949. Fax: (512) 471-6135. E-mail: m.hackert@mail.utexas.edu. (C.P.W.) Phone: (512) 471-6198. Fax: (512) 232-2606. E-mail: cwhitman@uts.cc.utexas.edu.

[1] Abbreviations: Ap, ampicillin; ARP, automated refinement procedure; BCA, bicinchoninic acid; 3-BP, 3-bromopyruvate; CHMI, 5-(carboxymethyl)-2-hydroxymuconate isomerase; DEAE, diethylaminoethyl; F_o, F_c, observed and calculated structure factors, respectively; HPLC, high-pressure liquid chromatography; IPTG, isopropyl-β-D-thiogalactoside; LB, Luria−Bertani medium; LPS, lipopolysaccharide; MIF, macrophage migration inhibitory factor; 4-OT, 4-oxalocrotonate tautomerase; PPT, phenylpyruvate tautomerase; SDS−PAGE, sodium dodecyl sulfate−polyacrylamide gel electrophoresis.

10.1021/bi9904048 CCC: $18.00
Published on Web 05/15/1999

4-oxalocrotonate tautomerase (4-OT) and 5-(carboxymethyl)-2-hydroxymuconate isomerase (CHMI) (*5*−*7*). Both 4-OT and CHMI share a common but an unusual catalytic strategy in that the amino-terminal proline serves as the catalytic base in the reaction shuttling a proton between C-3 and C-5 of **5** and **6** (Scheme 2) (*8*, *9*). Proline can act as a base in these

Scheme 2

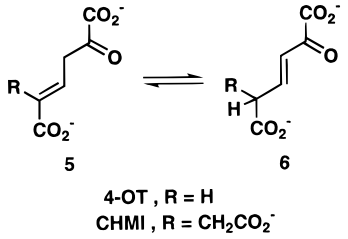

reactions because it is situated in a hydrophobic pocket lowering its pK_a to 6.4 (*10*). MIF has a similarly situated amino-terminal proline with a pK_a of ∼6.0, which has been implicated as the catalytic base in the MIF-catalyzed enolization of **1** to **2** by kinetic analysis, affinity labeling with 3-bromopyruvate, and NMR studies (*11*, *12*). In addition to Pro-1, there are four tyrosine residues (Tyr-36, Tyr-75, Tyr-95, and Tyr-98) and a lysine residue (Lys-32) within the proposed active-site region. Little is known about how these residues might function in the enzymatic reaction and what other active-site residues might be involved in the reaction.

The previous crystal structures of MIF were solved in the absence of a ligand (*5*, *6*). To obtain a better understanding of the catalytic mechanism, it would be highly desirable to have a crystal structure of MIF complexed with a ligand at the putative active site. Moreover, a detailed characterization of the interactions in such a structure would be of great value in the design of potential therapeutic agents if a link were established between the proinflammatory activities of MIF and the enzymatic activity. In view of the observation that MIF and PPT are the same protein, it was anticipated that the enol analogues of **2** and **4** shown in Scheme 3 might serve as potential ligands or as lead compounds for such ligands because these compounds are reportedly competitive inhibitors of PPT (*13*). Accordingly, we have been investigating the effect of these compounds on the enzymatic activity of MIF.

In the course of these studies, we found that one of these compounds, (*E*)-2-fluoro-*p*-hydroxycinnamate (**7**, Scheme 3),

Scheme 3

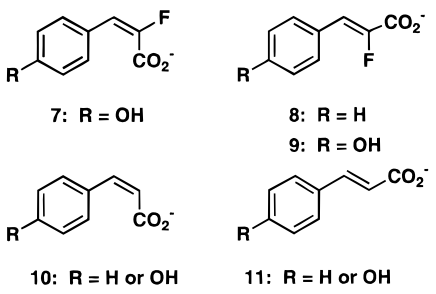

is a potent competitive inhibitor of the enzymatic activity of MIF with a $K_i = 2.6$ μM. More significantly, however, a crystal structure of mouse MIF complexed with **7** has been determined at 1.8 Å resolution. The structure presents a detailed picture of the interactions between **7** and the active-site residues of MIF and provides a structural basis for the observed differences in the potencies of the inhibitors shown in Scheme 3, the substrate specificity of MIF, and the stereochemistry of proton abstraction from C-3 of **1**. Moreover, a reaction mechanism for the enzymatic reaction catalyzed by MIF can be inferred from the geometry of the MIF·**7** complex. The tight binding of **7** to MIF also prompted an examination of whether MIF catalyzes the ketonization of **2** and **4** more efficiently than the enolization of **1** and **3**. The resulting k_{cat}/K_M values determined for **2** and **4** coupled with the "snug fit" observed between MIF and **7** in the crystal structure suggest that the physiologically relevant reaction catalyzed by MIF might be the ketonization of an enol substrate similar in structure to **2** or **4**. Thus, the combination of these findings sheds considerable light on the nature of inhibition and the catalytic mechanism of the reaction catalyzed by the enzymatic activity observed for MIF.

EXPERIMENTAL PROCEDURES

Materials. All biochemicals were purchased from Sigma Chemical Co. with the exception of (*E*)-2-fluoro-*p*-hydroxycinnamate (**7**), which was synthesized according to a literature procedure (*13*). The Amicon filtration cell and ultrafiltration membranes were purchased from Amicon. The clone containing recombinant murine MIF was obtained from Dr. Richard Bucala (The Picower Institute for Medical Research, Manhasset, NY).

General Methods. HPLC separations were performed on a Waters system using a Waters Protein Pak (DEAE−5PW) anion-exchange column. Protein concentrations were determined using the commercially available bicinchoninic acid (BCA) protein assay kit (Pierce Chemical Co., Rockford, IL). Protein was analyzed by sodium dodecyl sulfate−polyacrylamide gel electrophoresis (SDS−PAGE) under denaturing conditions on 12.5% gels (*14*). Kinetic data were obtained on a Hewlett-Packard 8452A Diode Array spectrophotometer and fitted by nonlinear regression data analysis using the Grafit program (Erithacus Software Ltd., Staines, U.K.) obtained from Sigma Chemical Co.

Purification of Recombinant MIF. MIF was purified by a previously described procedure with the following modifications (*12*). The active fractions eluting from the Waters Protein Pak (DEAE-5PW) anion-exchange column were pooled, concentrated, and loaded on a Sephadex G-75 gel filtration column (60 × 3 cm) equilibrated with 20 mM Tris buffer (pH 7.4) containing 20 mM NaCl. At a flow rate of 0.5 mL/min, the protein eluted after 5 h and was collected in five 2.5 mL fractions. MIF was purified in two separate runs using 3 mL of an 8 mg/mL solution in each run. The active protein was collected and concentrated to ∼16 mg/mL in an Amicon filtration cell. The subunit molecular mass of MIF was verified by electrospray ionization mass spectrometry (ESI-MS) using a LCQ Finnigan octapole electrospray mass spectrometer.

Enzymatic Activity Assays. The enolization of **1** and **3** by MIF was monitored by a previously described assay (*13*). The ketonization of **2** and **4** by MIF was monitored as follows. The disappearance of the enol of phenylpyruvic acid is followed at 288 nm ($\epsilon = 17\,300$ M^{-1} cm^{-1}) and the disappearance of the enol of (*p*-hydroxyphenyl)pyruvic acid

is followed at 300 nm ($\epsilon = 21\,600\ M^{-1}\ cm^{-1}$). The assay mixture contains 50 mM Na_2HPO_4 buffer (1 mL, pH 6.5) and an aliquot of a sufficiently dilute solution of MIF (0.5−1.0 μL of a 2.3 mg/mL solution so that the final concentration is 93−190 nM) to obtain an initial linear rate. The assay was initiated by the addition of a small quantity (1−3.3 μL) of either phenylpyruvic acid (**2**) or (*p*-hydroxyphenyl)pyruvic acid (**4**) from various stock solutions (5, 10, 20, or 50 mM) made up in ethanol. The concentration of substrate used to assay the enzymatic activity of MIF ranged 10−150 μM. No significant inhibition of the enzymatic activity by ethanol is observed at concentrations of ≤0.5% (v/v).

Inhibition Studies of MIF. The reversible competitive inhibition of MIF was examined at increasing concentrations of **7** (0, 1.0, 2.5, 5, and 10 μM) in the presence of 12 concentrations of **2** (10−150 μM). At each inhibitor concentration, a quantity of MIF (14 μL of a 1.1 mg/mL solution) was added to 14 mL of assay buffer (50 mM NaH_2PO_4 buffer, pH 6.5) and incubated for 1 h. Without the incubation period, the kinetic results were found not to be consistent. The concentrated protein solution may form aggregates, which may not readily break up upon dilution. After the incubation period, a sufficient quantity of **7** from a 10 mM stock solution made up in 50 mM NaH_2PO_4 buffer (pH 6.5) was added to the mixture to yield the desired final concentration of **7**. After 5 min, aliquots (1 mL) of the mixture were removed and assayed at the different concentrations of **2**. The kinetic data were fitted by nonlinear regression data analysis using the equation for competitive inhibition provided with the Grafit program.

Crystallization. MIF was cocrystallized in the presence of **7** using the hanging drop vapor diffusion method. Crystals were grown at 22 °C from 10 μL drops which contained 5 μL of MIF (16 mg/mL in 20 mM Tris buffer, pH 7.4, containing 20 mM NaCl) and 5 μL of the precipitant solution. The precipitant solution contained 30% poly(ethylene glycol) 8000 in 50 mM sodium phosphate buffer pH 7.0, 50 μL of a solution of **7** (10 mg/mL) made up in 100 mM Na_2HPO_4 buffer, pH 7.5, and a sufficient amount of water so that the total final volume was 500 μL. The addition of **7** to the Na_2HPO_4 buffer adjusted the pH to 6.8. The final concentration of (PEG) 8000 was 22%. Crystals appeared overnight and grew to full size of 0.2 × 0.2 × 0.25 mm in 2−3 weeks. The space group of the crystals is *R*3 with unit cell parameters $a = b = 99.53$ Å, $c = 105.69$ Å, $\alpha = \beta = 90°$, $\gamma = 120°$. A single trimer is found in the asymmetric unit with a Matthews' parameter of 2.7 Å^3/Da and a calculated solvent content of 54% (*15*).

Data Collection. Diffraction data were collected to 1.8 Å resolution from a single crystal of the complexed MIF using an RAXIS-IV image plate detector installed on a Rigaku RU200H rotating anode X-ray generator. The generator, equipped with a nickel foil filter (0.000 15 in), was operated at 5 kW (50 kV × 100 mA). Focusing mirrors were used to produce a collimated beam width of 0.3 mm at the crystal. A sweep of 116° of diffraction data was collected as a set of 58 images of 2.0° oscillations at 25 °C. The exposure time for each image was 30 min at a crystal-to-detector distance of 100 mm. The high intensity, low-resolution reflections in this data set showed a significant amount of white radiation streaking. Therefore, a second data set was collected from the same crystal, translated along the spindle axis, to obtain improved low-resolution data. The second data set was collected as a sweep of 100° of diffraction data comprised of 50 images of 2.0° oscillations at 25 °C. The exposure time for each image was 10 min at a crystal-to-detector distance of 250 mm. A 0.001 in. nickel filter was used to reduce the white radiation streaking and improve background measurement for low-resolution reflections during data processing. The high-resolution (8.0−1.8 Å) and the low-resolution (50.0−3.0 Å) data sets were indexed separately using the program DENZO (*16*) and scaled together using SCALA (*17*). The data set is 99.1% complete from 50.0 to 1.8 Å resolution. The crystal and data collection statistics are summarized in Table 1.

Table 1: Crystal and Diffraction Data Collection

Crystal Data	
space group unit	*R*3
cell dimensions (hexagonal indexing)	
a (Å)	99.53
b (Å)	99.53
c (Å)	105.69
Diffraction Data	
camera length (mm)	100,[a] 250[b]
number of images	58,[a] 50[b]
exposure time (min)	30,[a] 10[b]
oscillation angle (deg)	2.0
R_{sym} (%)	7.6 (33.0)[c]
total observations	207 686
unique reflections	35 875
resolution range (Å)	50.0−1.8
completenesss (%)	99.1 (97.1)
average $I/\sigma(I)$	5.3 (2.0)
redundancy	3.8 (2.9)

[a] High-resolution data collected in the resolution range of 8.0−1.8 Å using a 0.000 15 in. Ni filter. The low resolution data in this set were omitted due to white radiation streaking. [b] Low resolution data were collected in the resolution range of 50.0−3.0 Å using a 0.001 in. Ni filter to reduce white radiation streaking. The two data sets were indexed separately using DENZO (*16*) and scaled together using SCALA (*17*). [c] Numbers in parentheses are the values for the highest resolution bin of the data.

Structure Determination. The crystal structure was solved by the molecular replacement method using a 2.6 Å structure (*R*-factor = 20.1%, R_{free} = 24.5%) of the native murine MIF as a search model,[2] which was solved previously using the native human MIF (PDF entry 1MIF) (*6*). The cross-rotation and translation functions were calculated with AMORE (*18*) using data collected from 10.0 to 3.0 Å resolution. The rotation function gave 47 solutions with correlation coefficients (cc) ranging from 13.0 for the best solution to 6.6, using a trimer as the search model. The best solution resulting from the first translation function calculation had a cc of 47.0 and an *R*-factor of 41.2%. The translation solution was refined using the rigid body refinement function in AMORE to give a cc of 57.9 and *R*-factor of 37.4%.

Structure Refinement. The model for the crystal structure of MIF complexed with **7** was refined with a computer-based minimization alternated with manual rebuilding. All refinement was carried out with REFMAC (*19*) and X-PLOR, version 3.851 (*20*). The initial refinement steps included conjugate gradient minimization, simulated annealing, and individual *B*-factor refinement in X-PLOR (*21*). REFMAC was used in further refinement and for the production of σ_A-

[2] Taylor, A. B., and Hackert, M. L. (1998) unpublished results.

Table 2: Statistics for the Refined Model[a]

resolution range[b] (Å)	50.0 − 1.8
no. of reflections used	35 875
no. of protein atoms	2607
no. of inhibitor atoms	39
no. of water molecules	93
deviation in bond distances[c](Å)	0.016
deviation in bond angles[c]	1.7
deviation in dihedral angles[c]	27.4
deviation in improper torsions[c]	0.96
R-factor[d]	0.178
R_{free}[d]	0.227

[a] Refinement was performed with the X-PLOR package, version 3.851 (*20*), and with REFMAC (*19*). X-PLOR was used for the final stages of refinement. [b] The bulk solvent correction implemented in the X-PLOR package was applied to the entire resolution range of data used in the refinement (*26*). [c] Root-mean-square deviations from the "ideal" values in the X-PLOR protein_rep.param parameter set. [d] *R*-factor calculations are based on all data including a bulk solvent correction. A test set of 5% of the data (1792 reflections) was used for the R_{free} calculation (*24*).

Table 3: Kinetic Parameters for MIF with Various Substrates[a]

substrate	K_m (μM)	k_{cat} (s^{-1})	k_{cat}/K_m (M^{-1} s^{-1})
1	4900 ± 1000	285 ± 40	5.8×10^4
2	130 ± 20	290 ± 30	2.2×10^6
3	2770 ± 430	120 ± 10	4.3×10^4
4	170 ± 40	160 ± 20	9.4×10^5

[a] The steady-state kinetic parameters were determined at 23 °C. Errors are standard deviations.

weighted $2F_o - F_c$ and $F_o - F_c$ maps used in the manual rebuilding process (*19*, *22*). The maps were displayed in the graphics package O (*23*), which was used for model rebuilding. Energy parameter files for the inhibitor, **7**, were created with the XPLO2D program (*24*). Solvent molecules were added with the automated process implemented by ARP (*25*). Noncrystallographic symmetry restraints were not necessary because the observation-to-parameter ratio is 3.2:1 for all reflections greater than 3.0σ. X-PLOR was used in the final refinement steps including the bulk solvent correction (*26*). The refinement statistics are summarized in Table 2.

RESULTS

Kinetic Studies of MIF. The kinetic properties of the enzymatic activity of MIF were determined by following the enolization of **1** and **3** and the ketonization of **2** and **4**. The steady-state kinetic parameters are summarized in Table 3. The data clearly show that the enol compounds (**2** and **4**) are better substrates than the keto compounds (**1** and **3**), as assessed by the differences in the k_{cat}/K_m values. There is a 38-fold increase in k_{cat}/K_m for **2** compared to **1** (resulting from the 38-fold decrease in K_m) and a 22-fold increase in k_{cat}/K_m for **4** compared to **3** (resulting primarily from the 16-fold decrease in K_m). In addition, (*E*)-2-fluoro-*p*-hydroxycinnamate (**7**) was examined as a potential competitive inhibitor of the enzymatic activity of MIF. It was found to be a competitive inhibitor of the enzymatic activity of MIF with a $K_i = 2.6 \pm 0.3$ μM.

Description of the Crystal Structure. The structure of the MIF complexed with **7** has been solved by the molecular replacement method and refined against 1.8 Å resolution data to a crystallographic *R*-factor of 17.8% and an R_{free} of 22.7%. The structures of the free MIF (human and rat) have previously been described as a trimer consisting of three identical subunits (*5*, *6*). Each subunit consists of a four-stranded β-sheet with two antiparallel α-helices on one side (*5*, *6*). The $2F_o - F_c$ maps used in model rebuilding of the complexed MIF structure showed continuous electron density for the entire polypeptide backbones of all three subunits in the asymmetric unit. In addition, strong, flat electron density was observed for the inhibitor molecule in a region near three residues (Pro-1, Tyr-95′, and Lys-32) previously identified as active-site residues (Figure 1) (*30*). The structures of the free murine MIF and murine MIF·**7** complex are nearly identical, with a root-mean-square deviation of 0.34 Å for the Cα positions after superposition.

The Active Site. The region around Pro-1 in the free rat MIF crystal structure was first postulated to be the active site because of the protein's structural homology with the two bacterial isomerases, 4-OT and CHMI, which use Pro-1 as the catalytic base (*5*). It was further noted that Pro-1 of MIF is surrounded by several aromatic residues (Tyr-36, Tyr-

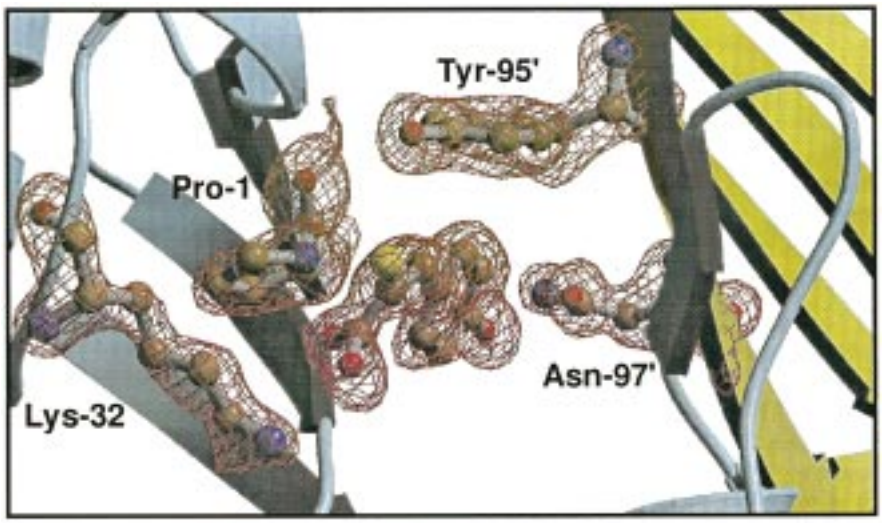

FIGURE 1: The $F_o - F_c$ simulated-annealing omit map of one active site showing the bound inhibitor. The map was calculated from 50.0 to 1.8 Å resolution using X-PLOR (*27*) and contoured at 3.0σ. The inhibitor interacts with Pro-1 and Lys-32 from one monomer, and with Tyr-95′ and Asn-97′ from the adjacent monomer as described in the text. The figure was prepared using BOBSCRIPT (*28*) and RASTER3D (*29*).

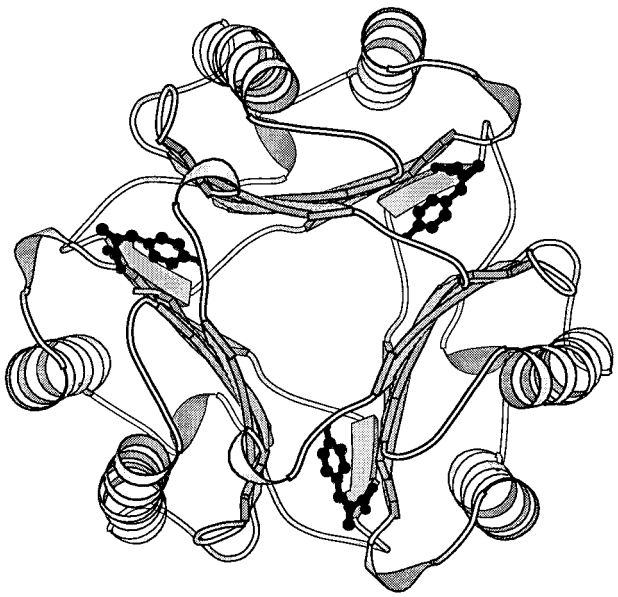

FIGURE 2: A ribbon diagram of the MIF trimer viewed down the molecular 3-fold axis showing the binding of **7**, a competitive inhibitor, and thereby confirming the location of the three active sites. Each inhibitor molecule interacts with residues from adjoining subunits suggesting that an active site is composed of residues from adjacent monomers. The figure was prepared with MOLSCRIPT (*31*).

75, Tyr-95, and Tyr-98 as well as Phe-49 and Phe-113) forming a hydrophobic pocket. The amino-terminal proline in 4-OT and in CHMI is also located at the base of a hydrophobic pocket although the pocket is formed by different residues. In the crystal structure of MIF complexed with the competitive inhibitor **7**, there is a well-defined region of electron density at each interface between neighboring subunits (Figure 2). The electron density clearly corresponds to **7** and confirms the location of the active site. The structure also shows that **7** interacts with residues from the two adjacent subunits suggesting that the active site is comprised of residues from two neighboring subunits (Figure 2). Likewise, the active site of 4-OT is proposed to be located at the interface of two adjacent dimers where one 4-OT dimer is structurally equivalent to one MIF monomer (*7*).

Interaction of 7 with Active-Site Residues. Examination of the molecular surface of the active-site region in the crystal structure of the MIF·**7** complex reveals that the inhibitor fits "snugly" within a narrow tunnel-like cavity (Figure 3).[3] The hydroxyl group on the phenyl ring is at the back of the cavity and the carboxylate group is at the mouth of the cavity. There are several interactions within this cavity that can account for the tight binding of **7** (Figure 4). One carboxylate oxygen of **7** is within 2.9 Å of the ammonium group of Lys-32, which is positioned in an extended form. The other carboxylate oxygen is within 2.4 Å of the nitrogen of Pro-1. The hydroxyl group of **7** is within hydrogen-bonding distance of the carbonyl oxygen of Asn-97′ (2.7 Å). There may also be a weak interaction between the fluorine of **7** and the hydroxyl group of Tyr-95′ (3.6 Å). Finally, the phenyl group of **7** is bound in a hydrophobic pocket formed by the side chains of Met-2, Ile-64, Met-101, Val-106, and Phe-113 and the phenyl ring of Tyr-95′. Pro-1 and Lys-32 are derived from one monomer while Tyr-95′ and Asn-97′ are from the

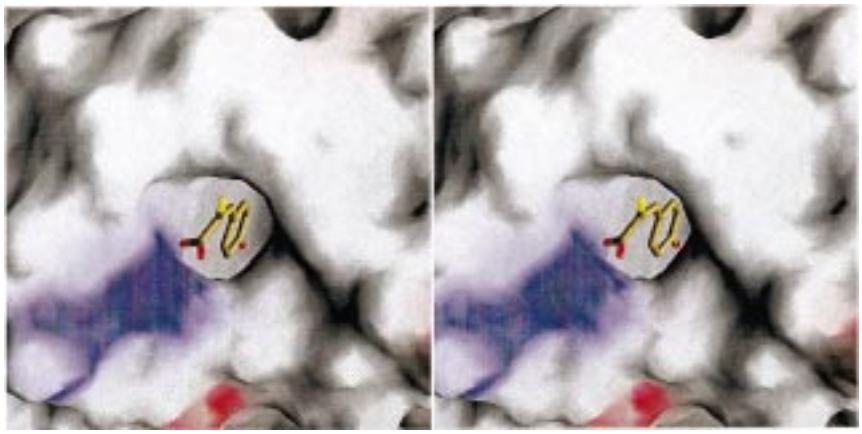

FIGURE 3: A molecular surface stereo-diagram illustrating the narrow active site cavity of MIF occupied by the inhibitor. The blue and red shading represent the electrostatic field potential contributed by either a cationic (blue) and an anionic (red) residue. The blue patch on the surface of MIF near the carboxylate group of **7** corresponds to Lys-32. The figure was produced using GRASP (*32*).

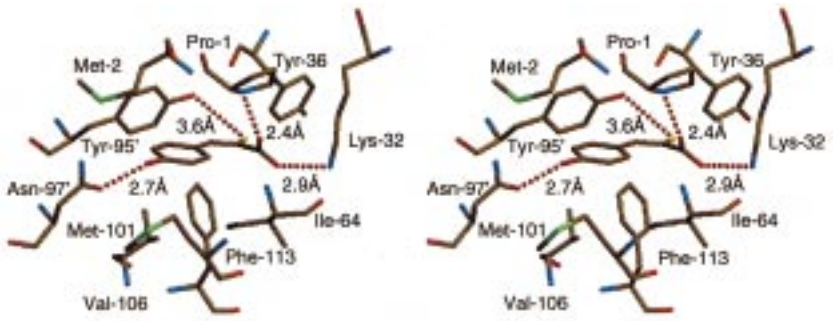

FIGURE 4: A stereodiagram showing specific interactions between **7** and the active-site residues of MIF. The tight binding of **7** is presumably due to its interactions with Met-2, Lys-32, Ile-64, Tyr-95′, Asn-97′, Met-101, Val-106, and Phe-113. Distances are measured from center to center of the two atoms.

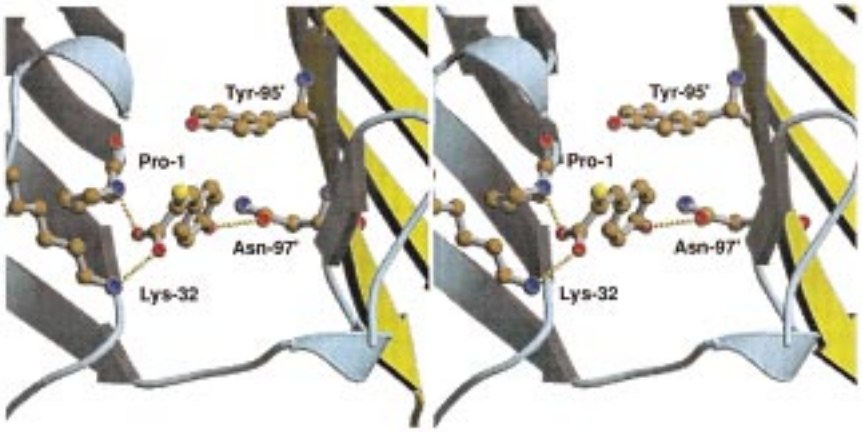

FIGURE 5: A stereodiagram showing the interaction of **7** with active-site residues contributed from two MIF monomers. The inhibitor interacts with Pro-1 and Lys-32 from one monomer, and with Tyr-95′ and Asn-97′ from the adjacent monomer. The dotted lines indicate that the atoms are within hydrogen bonding distance. The figure was prepared using RASTER3D (*29*) and MOLSCRIPT (*31*).

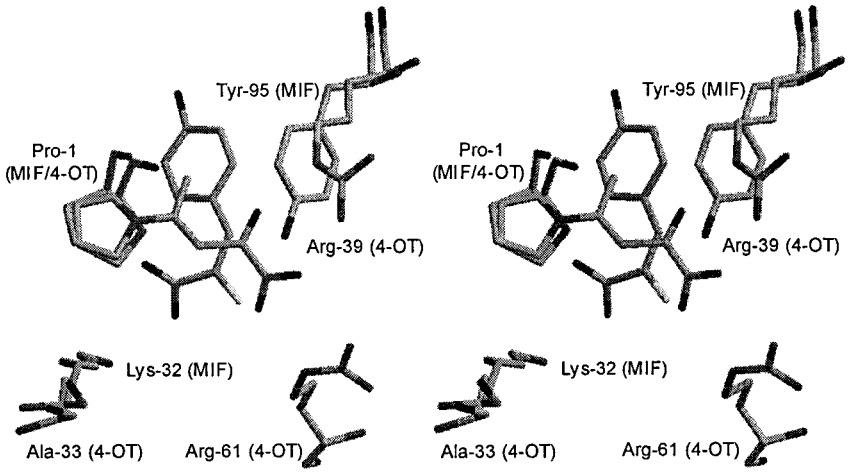

FIGURE 6: A stereodiagram showing the superimposition of the crystal structures of the key active site residues in the MIF·**7** complex and in the complex of 4-OT inactivated by 2-oxo-3-pentynoate. The putative general acid catalyst in 4-OT, Arg-39, aligns with Tyr-95 in MIF. The residues responsible for binding the C-1 carboxylate groups (Arg-61 in 4-OT and Lys-32 in MIF) do not align. The figure was prepared using RASTER3D (*29*) and MOLSCRIPT (*31*).

neighboring subunit (Figure 5). The major residues responsible for the binding of the phenyl moiety (Met-2, Ile-64, Met-101, Val-106, and Phe-113) are from the same subunit as Pro-1 and Lys-32.

Within this narrow cavity, Pro-1 is positioned above the plane of **7**. The nitrogen of Pro-1 is 3.3 Å from C-3 of **7**. If **7** were replaced with **1**, Pro-1 is in a position to remove the *pro-R* hydrogen and to generate the E-isomer of **2**. It has been previously determined that the PPT-catalyzed enolization of **1** results in the abstraction of the *pro-R* hydrogen (*13*, *33*). This observation suggests that **7** and the substrate bind comparably in the active site.

Three other residues (Tyr-36, Tyr-75, and Tyr-98) were previously identified as active-site residues on the basis of their proximity to Pro-1 in the crystal structure of MIF solved in the absence of a ligand (*5*, *30*). The distance between **7** and one of these three residues in the MIF·**7** complex rules out any appreciable interaction. Of the three, Tyr-36 is the closest to **7** but its hydroxyl group is still over 6 Å from the fluorine.

Superimposition of the Active Sites of the MIF·7 Complex and the 2-Oxo-pentynoate-inactivated 4-OT Complex. 4-OT, CHMI, and MIF have been categorized as members of an enzyme superfamily because they are structurally homologous and they utilize Pro-1 as the general base catalyst (*7*). In the 4-OT-catalyzed reaction, Arg-39 has been implicated as the general acid catalyst (*8*). The positioning of Arg-39 in a recent crystal structure of 4-OT inactivated by 2-oxo-3-pentynoate supports this contention (*34*). Superimposition of the active sites of MIF and 4-OT with their respectively bound ligands aligns Arg-39 of 4-OT with Tyr-95′ of MIF (Figure 6). Moreover, of the three nitrogens in the side chain of Arg-39, the side chain ϵ-nitrogen, which is within 2.9 Å of the C-2 carbonyl oxygen of the bound adduct and therefore may provide a crucial interaction for catalysis, is the one most directly aligned with the hydroxyl group of Tyr-95′. In contrast, the alignment of these structures shows that the carboxylate groups of the bound ligands are pointing in nearly opposite directions. This would suggest that the residues responsible for the binding of the C-1 carboxylate groups do not align. In the 4-OT structure, Arg-61 interacts

[3] Although there are ordered water molecules in the active site region of the crystal structure of the free human MIF, the structure of the murine MIF·**7** complex contains only the inhibitor (*6*). Presumably, any bound water molecules in the structure are displaced upon binding of the inhibitor.

with this carboxylate group while, in the MIF structure, Lys-32 interacts with the C-1 carboxylate group of **7**. Lys-32 in MIF aligns with Ala-33 in 4-OT, which does not play a role in the binding of the inhibitor. Using the least-squares method in O (*23*) to superimpose the Pro-1 residues of both structures, Tyr-95′ onto Arg-39 of 4-OT, and Lys-32 onto Ala-33 in 4-OT, there is a root-mean-square deviation of 0.56 Å for the Cα atoms. Arg-61 of 4-OT does not have an MIF counterpart in the structural alignment.

DISCUSSION

The results of crystallographic and kinetic studies provide new insights into the nature of catalysis and inhibition of the enzymatic activity exhibited by MIF. Examination of the crystal structure of the MIF·**7** complex reveals the structural basis for the tight binding of **7** and the analogous compounds shown in Scheme 3. If these same interactions are used in the MIF-catalyzed enzymatic reaction, then a structural basis for the substrate specificity, the molecular basis for the stereochemical course of the reaction, and a plausible reaction mechanism can be inferred from the structure. In addition, the highly complementary fit between the active-site cavity of MIF and **7** suggests that the physiologically relevant reaction for MIF involves the ketonization of an enol compound. Finally, these results define further similarities and differences in the active sites of MIF and the two other members of this superfamily, 4-OT and CHMI.

The enol fluoride, **7**, is one in a series of chemically stable enol analogues (Scheme 3) previously reported to be competitive inhibitors of PPT with widely varying potency as reflected by the different values of K_i. On the basis of the inhibition data, three structural features of these compounds were correlated with the binding potency (*13*). First, the stereochemistry of the compound is critical. The more potent inhibitors are those compounds in which the phenyl and the carboxylate group are on the same side of the double bond (*E*-**7** or *Z*-**10**). The crystal structure clearly shows that, in this position, there is a strong interaction between the carboxylate oxygens and Lys-32 and Pro-1. This orientation places the phenyl group of the inhibitor in a position to interact with the hydrophobic side chains of Met-2, Ile-64, Met-101, Val-106, and Phe-113 and with the phenyl ring of Tyr-95′. Second, the p-hydroxy derivatives (e.g., **9**) are more potent inhibitors than their non-hydroxylated counterparts (e.g., **8**). It was proposed that the greater potency of these compounds was due to the presence of a hydrogen bond acceptor in the active site of PPT. This prediction is borne out by the crystal structure which shows an interaction between the carbonyl oxygen of Asn-97′ and the p-hydroxy group. Finally, the vinyl fluoride derivatives (**7**) are not significantly more potent inhibitors than the corresponding vinyl compounds (**10**, where R = OH). The crystal structure shows an interaction between the hydroxy group of Tyr-95′ and the fluoride substituent, but the distance between these groups (3.6 Å) does not suggest a strong interaction.

Although MIF clearly exhibits a phenylpyruvate tautomerase activity, questions have been raised about whether phenylpyruvate is the actual physiological substrate (*4*, *11*). The primary reason for these questions is due to the low values of k_{cat}/K_m ($\sim 10^4$) measured for **1** and **3**. Moreover, there is no obvious physiological function for a phenylpyruvate tautomerase activity (*11*). In view of these questions, it was initially anticipated that if another substrate did exist, then the crystal structure of the MIF·**7** complex might suggest the features of such a molecule. However, an examination of the structure shows that **7** fits quite snugly within the cavity, leaving little room for any additional substitution.

This intimate fit and two other observations suggested that MIF might process **2** and **4** more efficiently than either **1** or **3**. First, the value of K_i measured for **7** is $\sim 10^3$-fold less than the values of K_m measured for **1** or **3**. Moreover, several of the enol analogues shown in Scheme 3 have K_i values that are also $\sim 10^2-10^3$ less than these K_m values (*13*). Second, the structurally homologous proteins, 4-OT and CHMI, ketonize dienolic substrates quite efficiently (*9*, *36*).[4]

The results of kinetic studies investigating this issue demonstrate that MIF processes **2** and **4** (the enol isomers) more efficiently than either **1** or **3** (the corresponding keto isomers) as assessed by the values k_{cat}/K_m. This observation is consistent with the Haldane relationship, which places a constraint on the relative values of k_{cat}/K_m measured for the forward and reverse reactions (*38*). Because the predominant product at equilibrium is the keto isomer (*33*), the value of k_{cat}/K_m measured in the enol to keto direction should be greater than that measured in the keto to enol direction. The primary reason for the increase in the values of k_{cat}/K_m is the significant decrease in the values of K_m for **2** and **4**, which may be due, in part, to the tighter binding of the enol isomers.

The interactions governing the binding of **1**-**4** within the active-site cavity of MIF can be reasonably inferred from the crystal structure of the MIF·**7** complex. Accordingly, the p-hydroxy group on substrates **3** and **4** will interact with Asn-97′ while one of the oxygens of the C-1 carboxylate group of **1**−**4** will interact with Lys-32. The residue responsible for the binding of the other carboxylate oxygen is not known, but it is unlikely to be Pro-1 because this residue is the general base catalyst (*11*, *12*). The carbonyl oxygen of **1** and **3** and the enol oxygen of **2** and **4** may have a weak interaction with the hydroxyl group of Tyr-95′. The phenyl group of substrates **1**-**4** presumably interacts with the hydrophobic side chains of Met-2, Ile-64, Met-101, Val-106, and Phe-113, and with the phenyl ring of Tyr-95′.

In view of these interactions, a structural basis for the different kinetic parameters obtained for **1**−**4** (Table 3) can be postulated. The most striking difference is the one between the K_m values obtained for the keto isomers (**1** and **3**) and those obtained for the enol isomers (**2** and **4**). A combination of factors may be responsible for the much greater affinity of the enol isomers for the active site. Among these factors are the increased planarity, the decreased conformational mobility, and the preferred E-stereochemistry (*13*). Presumably, these features enable the enol isomers to interact more favorably with their respective binding residues at the active site. A second difference is the one between the K_m value determined for the two keto isomers **1** (K_m = 4.9 mM) and **3** (K_m = 2.8 mM). This difference may be partially due to a greater affinity of **3** for the active site because of the interaction between its p-hydroxy group and Asn-97′. It is unknown why there is not a similar difference between the K_m values of the enol isomers (**2** and **4**) even though the

[4] The free acids of both **2** and **4** exist solely as their enol isomers in the crystalline state (*37*).

presence of a p-hydroxy group significantly increases the potency of the inhibitors (as judged by the decrease in K_i) (*13*). Interestingly, the p-hydroxy group on **3** and **4** (and presumably, the interaction with Asn-97′) reduces the turnover of these substrates as indicated by the diminished values of k_{cat}. There are two possible explanations for this observation. The interaction between the p-hydroxy group and Asn-97′ may place the substrate in a position such that it is not optimally aligned with the general base and general acid catalysts. This assumes that proton abstraction is rate limiting. Alternatively, the interaction between the p-hydroxy group and Asn-97′ may limit the rate of the release of product.

The interactions proposed to be responsible for the binding of substrates **1**−**4** also provide a structural basis for the observed stereochemistry of the reaction. Retey et al. (*33*) showed experimentally that PPT removes the *pro-R* hydrogen of **1** and **2** while Pirrung et al. (*13*) argued that the enzyme generates the E-isomer of **4** from **3**. Pro-1 sits above the plane of **1** or **3,** where it is in a position to remove the *pro-R* proton at C-3 and generate the E-isomer of either **2** or **4**. Likewise, Pro-1 sits above the plane of **2** or **4** where it can deliver a proton to the *re*-face to afford either **1** or **3**.

The geometry of the MIF·**7** complex suggests the mechanism for catalysis shown in Scheme 4. In this mechanism,

Scheme 4

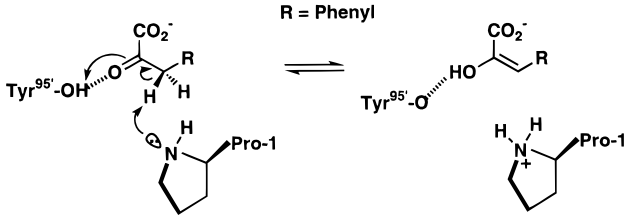

Pro-1 acts as the general base to abstract the *pro-R* proton of **1** or **3** while Tyr-95′ may be in a position to stabilize the developing negative charge on the carbonyl oxygen. One concern about this mechanism is that the crystal structure of the MIF·**7** complex does not place Tyr-95′ within hydrogen-bonding distance of the carbonyl oxygen. If Tyr-95′ does not act as the general acid catalyst in the reaction, an examination of the crystal structure does not reveal any other polar groups in the active site that can serve in this capacity. If MIF uses general acid−base catalysis, as do other nonmetal dependent keto−enol isomerases (*39*, *40*), then this crystal structure suggests that the protein will have to undergo a conformational change upon substrate binding in order to bring another residue into position to act as a general acid catalyst. The function of Tyr-95′ in the mechanism is under investigation.

The structural and mechanistic similarities between MIF and two bacterial isomerases, 4-OT and CHMI, suggest that these proteins are members of a superfamily that diverged from a common ancestral protein catalyzing the keto−enol tautomerization of a pyruvyl moiety (*7*, *12*). Comparing the crystal structures of 4-OT and MIF with bound ligands delineates the characteristics of this superfamily further. It has already been established that 4-OT, MIF, and CHMI have the same overall fold and that Pro-1 is the general base catalyst (*7*). The crystal structure of 4-OT inactivated by 2-oxo-3-pentynoate (2-OP) suggests that the active site is located at the interface of adjacent subunits and is composed of residues from both. The active site of MIF is formed similarly. In both structures, the putative general acid catalyst is located in one subunit while the general base catalyst is located in the adjacent subunit. There are also similarities in the substrates processed by MIF, 4-OT, and CHMI. Previous studies have shown that 4-OT and CHMI efficiently catalyze the ketonization of a dienolic compound (*35*, *36*). MIF also catalyzes the ketonization of an enol compound with a high degree of efficiency. There are also some differences. Although Pro-1 is used as the general base in both mechanisms, different residues are involved in binding and in other aspects of catalysis. In 4-OT, it is proposed that Arg-39 and an ordered water molecule stabilize the developing negative charge on the carbonyl oxygen (*34*), whereas in MIF, Tyr-95 serves in this capacity. A more striking difference between these two proteins is the different manner in which the C-1 carboxylate groups of the substrates may bind to the active sites. In 4-OT, Arg-61 in the C-terminal loop forms a bidentate interaction with the C-1 carboxylate group. This led to the suggestion that a conformational change brings Arg-61 into the active site upon substrate binding (*34*). In MIF, the C-1 carboxylate group is presumed to interact with Lys-32, which is found within the active site region. From this observation, it can be inferred that the binding of substrate does not induce a conformational change. Further study is necessary to determine whether these observations accurately reflect the binding of substrate.

ACKNOWLEDGMENT

We are grateful to Dr. R. Bucala for providing us with the clone containing recombinant mouse MIF. Electrospray ionization mass spectrometry was performed by the analytical instrumentation service core supported by Center grant ES 07784.

REFERENCES

1. Bucala, R. (1996) *FASEB J. 10*, 1607−1613.
2. Calandra, T., Bernhagen, J., Metz, C. N., Spiegel, L. A., Bacher, M., Donnelly, T., Cerami, A., and Bucala, R. (1995) *Nature 377*, 68−71.
3. Bernhagen, J., Mitchell. R. A., Calandra, T., Voelter, W., Cerami, A., and Bucala, R. (1994) *Biochemistry 33*, 14144−14155.
4. Rosengren, E., Aman, P., Thelin, S., Hansson, C., Ahlfors, S., Bjork, P., Jacobsson, L., and Rorsman, H. (1997) *FEBS Lett. 417*, 85−88.
5. Suzuki, M., Sugimoto, H., Nakagawa, A., Tanaka, I., Nishihira, J., and Sakai, M. (1996) *Nat. Struct. Biol. 3*, 259−266.
6. Sun H.-W., Bernhagen, J., Bucala, R., and Lolis, E. (1996) *Proc. Natl. Acad. Sci. U.S.A. 93*, 5191−5196.
7. Murzin, A. G. (1996) *Curr. Opin. Struct. Biol. 6*, 386−394.
8. Subramanya, H. S., Roper, D. I., Dauter, Z., Dodson, E. J., Davies, G. J., Wilson, K. S., and Wigley, D. B. (1996) *Biochemistry 35*, 792−802.
9. Stivers, J. T., Abeygunawardana, C., Mildvan, A. S., Hajipour. G., Whitman, C. P., and Chen, L. H. (1996) *Biochemistry 35*, 803−813.
10. Stivers, J. T., Abeygunawardana, C., Mildvan, A. S., Hajipour. G., and Whitman, C. P. (1996) *Biochemistry 35*, 814−823.
11. Swope, M., Sun H.-W., Blake, P., and Lolis, E. (1998) *EMBO J. 17*, 3534−3541.
12. Stamps, S. L., Fitzgerald, M. C., and Whitman, C. P. (1998) *Biochemistry 37*, 10195−10202.
13. Pirrung, M. C., Chen, J., Rowley, E. G., and McPhail, A. T. (1993) *J. Am. Chem. Soc. 115*, 7103−7110.
14. Laemmli, U. K. (1970) *Nature 227*, 680−685.
15. Matthews, B. W. (1968) *J. Mol. Biol.* 33, 491−497.

16. Otwinowski, Z., and Minor, W. (1996) *Methods Enzymol. 276*, 307−326.
17. Evans, P. R. (1993) *Proceedings of CCP4 Study Weekend on Data Collection & Processing*, pp 114−122, Daresbury Laboratory, Warrington, U.K.
18. Navaza, J. (1994) *Acta Crystallogr., Sect. A 50*, 157−163.
19. Murshudov, G. N., Vagin, A. A., and Dodson, E. J. (1997) *Acta Crystallogr., Sect. D 53*, 240−255.
20. Brunger, A. T., Kuriyan, J., and Karplus, M. (1987) *Science 235*, 458−460.
21. Brunger, A. T., Krukowski, A., and Erickson, J. (1990) *Acta Crystallogr., Sect. A 46*, 585−593.
22. Read, R. J. (1986) *Acta Crystallogr., Sect. A 42*, 140−149.
23. Jones, A. T., Zou, J. T., Cowan, S. W., and Kjeldgaard, M. (1991) *Acta Crystallogr., Sect. A 47*, 110−119.
24. Kleywegt, G. J. (1995) *CCP4/ESF-EACBM Newsl. Protein Crystallogr. 31*, 45−50.
25. Lamzin, V. S., and Wilson, K. S. (1997) *Methods Enzymol. 277*, 269−305.
26. Jiang, J.-S., and Brunger, A. T. (1994) *J. Mol. Biol. 243*, 100−115.
27. Hodel, A., Kim, S.-H., and Brunger, A. T. (1992) *Acta Crystallogr., Sect. A 48*, 851−859.
28. Esnouf, R. M. (1997) *J. Mol. Graphics 15*, 132−134.
29. Merritt, E. A., and Bacon, D. J. (1997) *Methods Enzymol. 277*, 505−524.
30. Suzuki, M., Sugimoto, H., Tanaka, I., and Nishihira, J. (1997) *J. Biochem. 122*, 1040−1045.
31. Kraulis, P. J. (1991) *J. Appl. Crystallogr. 24*, 946−950.
32. Nicholls, A., Sharp, K. A., and Honig, B., (1991) *Proteins: Struct., Funct., Genet. 11*, 281−296.
33. Retey, J., Bartl, K., Ripp, E., and Hull, W. E. (1977) *Eur. J. Biochem. 72*, 251−257.
34. Taylor, A. B., Czerwinski, R. M., Johnson, W. H., Jr., Whitman, C. P., and Hackert, M. L. (1998) *Biochemistry 37*, 14692−14700.
35. Whitman, C. P., Aird, B. A., Gillespie, W. R., and Stolowich, N. J. (1991) *J. Am. Chem. Soc. 113*, 3154−3162.
36. Hajipour, G., Johnson, W. H., Dauben, P. D., Stolowich, N. J., and Whitman, C. P. (1993) *J. Am. Chem. Soc. 115*, 3533−3542.
37. Larsen, P. O., and Wieczorkowska, E. (1974) *Acta Chem. Scand. B 28*, 92−96.
38. Fersht, A. R. (1985) *Enzyme Structure and Mechanism*, 2nd ed., pp 112−113, W. H. Freeman and Co., San Francisco.
39. Harris, T. K., Cole, R. N., Comer, F. I., and Mildvan, A. S. (1998) *Biochemistry 37*, 16828−16838.
40. Wu, Z. R., Ebrahimian, S., Zawrotny, M. E., Thornburg, L. D., Perez-Alvarado, G. C., Brothers, P., Pollack, R. M., and Summers, M. F. (1997) *Science 276*, 415−417.

BI9904048